1975ApJ...197..415K

THE ASTROPHYSICAL JOURNAL, 197:415–424, 1975 April 15
© 1975. The American Astronomical Society. All rights reserved. Printed in U.S.A.

THE ENVELOPES OF TYPE II SUPERNOVAE

ROBERT P. KIRSHNER
Hale Observatories, California Institute of Technology and
Carnegie Institution of Washington

AND

JOHN KWAN
Institute for Advanced Study
Received 1974 September 9

ABSTRACT

Absolute spectral energy distributions of Type II supernovae have been used to derive a consistent physical picture of their ejected envelopes. Continuum observations are consistent with a photosphere that expands to a radius of 10^{15} cm and then begins to shrink at nearly constant temperature. The hydrogen recombination implies an electron density which decreases from 10^{10} to 2×10^{7} cm^{-3} in a time of 400 days. A total hydrogen mass in excess of 1 $M_{\odot}$ is required to prevent rapid recombination in the envelope.

The Ca II lines at λλ8600 and 7300 are produced collisionally: an explicit calculation of the emissivity demonstrates that the line ratios and strengths are consistent with solar abundances, a total mass of a few solar masses, and the electron density derived from hydrogen recombination. Similarly, the [O I] λ6300 emission is consistent with this general picture.

A quantitative analysis of line optical depths confirms the identifications of Na I λ5890, Mg I λ5174, and the Fe II blends near λλ4600 and 5100. A possible identification of K I λ7677 is suggested, while other candidates are rejected.

Subject headings: Ca II emission — spectrophotometry — supernovae

I. INTRODUCTION

Since 1969, the multichannel spectrometer (MCSP) attached to the 5-m Hale reflector has been used to obtain photometric scans of supernovae. Some of these data have recently been published by Kirshner *et al.* (1973) (hereinafter referred to as KOPS). In the present paper, the aim is to infer from these observations, some new ones, and the identifications of lines, reasonable estimates of the electron density, ionization, and elemental abundances in the envelopes of Type II supernovae. This is done through determination of the photospheric radius and temperature, the study of hydrogen recombination, and the study of line formation in the envelope.

The general picture is of a differentially expanding gas, with mass of about 3 $M_{\odot}$, and abundances similar to those in the Sun. Some unusual problems in the recombination of hydrogen are encountered; but these, like the peculiar line ratios of Ca II, can be shown to be consistent with this general picture. The line identifications of Na I, Mg I, Fe II, and [O I] are substantiated, and shown to be in quantitative agreement with this view. Other possible line identifications are considered in a systematic way.

The results are consistent with the lines that are seen, and their strengths; they explain the absence of others, and lead to possible identifications for still other lines.

For example, the identification of the Hα emission provides information about the electron density, and the population of the $n = 2$ level. This result is consistent with the observed Balmer decrement. Similarly, the electron density, together with the proposed identification of the Ca II λ7300 line, is consistent with the observed ratios of Ca II H and K, λ8600, and λ7300 lines. These problems and others leading to a simple picture of the physical conditions in the envelopes of Type II supernovae are discussed in the following sections.

II. OBSERVATIONS

Three Type II supernovae have been studied: SN 1969l in NGC 1058, SN 1970g in M101 (NGC 5457), and SN 1973r in NGC 3627. MCSP data for SN 1969l and SN 1970g are shown in KOPS, and spectroscopic data are available from Ciatti, Rosino, and Bertola (1971), Barbon, Ciatti, and Rosino (1973), and Kirshner and Kwan (1974).

Image-tube spectra and MCSP scans of SN 1973r in NGC 3627 are listed in table 1. The scans, with bandwidths of 40 Å for $\lambda < 5640$ Å and 80 Å for $\lambda > 5640$ Å are made without gaps over the entire observed wavelength range and are illustrated in figure 1. Observations between λ8900 and λ9700 have been deleted due to strong water vapor absorption in the Earth's atmosphere. The spectral energy distributions are based on the absolute calibration of α Lyrae given by Oke and Schild (1970).

Distances to NGC 1058 and M101 derived from supernova scans are 12 Mpc and 6 Mpc, respectively (Kirshner and Kwan 1974). A distance of 12 Mpc to NGC 3627 has been assumed, based on its radial velocity.

© American Astronomical Society • Provided by the NASA Astrophysics Data System

1975ApJ...197..415K

TABLE 1

OBSERVATIONS OF SN 1973r IN NGC 3627

Date (UT)	Julian Date −2,440,000	Plate	Observer	Dispersion or Channel Width	Useful Wavelength Range (Å)
1973 Dec. 31.....	2046	Q4685	Sandage	190 Å mm^{-1}	3900–6100
		Q4686	Sandage	190	3900–6100
		Q4687	Sandage	190	3900–6100
1974 Jan. 15.....	2061	MCSP	Oke	40/80 Å	3500–11000
1974 Jan. 18.....	2064	Q4723	Sandage	190	4400–6600
		Q4724	Sandage	190	4000–6700
		Q4725	Sandage	190	4000–6700
1974 April 26.....	2163	MCSP	Oke	40/80	3800–900

III. CONTINUUM MEASURES

The scans show that a continuum is present throughout the first year of expansion: the continua are supposed to be blackbodies. In view of the uncertainties in the distribution of the temperature and continuous opacity in the ejected gas, no more detailed model seems justified. However, the blackbody which fits best over the interval 10,000–5000 Å lies well above the observed flux from the supernova shortward of λ4000. Table 2 shows the best fits to the temperatures, and the radii required to give the observed flux density. Reddening has been included in the temperature estimates for 1970g and 1973r.

The notable fact is that, after initial expansion and cooling, the temperature at the photosphere seems to remain very nearly constant from age 1 month to 14 months. The observed decrease in flux density is attributed to shrinkage of the photosphere. This shrinkage is the inevitable result of a finite mass: as the envelope continues to expand, the outer layers become transparent in the continuum and eventually the photosphere retreats, despite the outward motion of the gas.

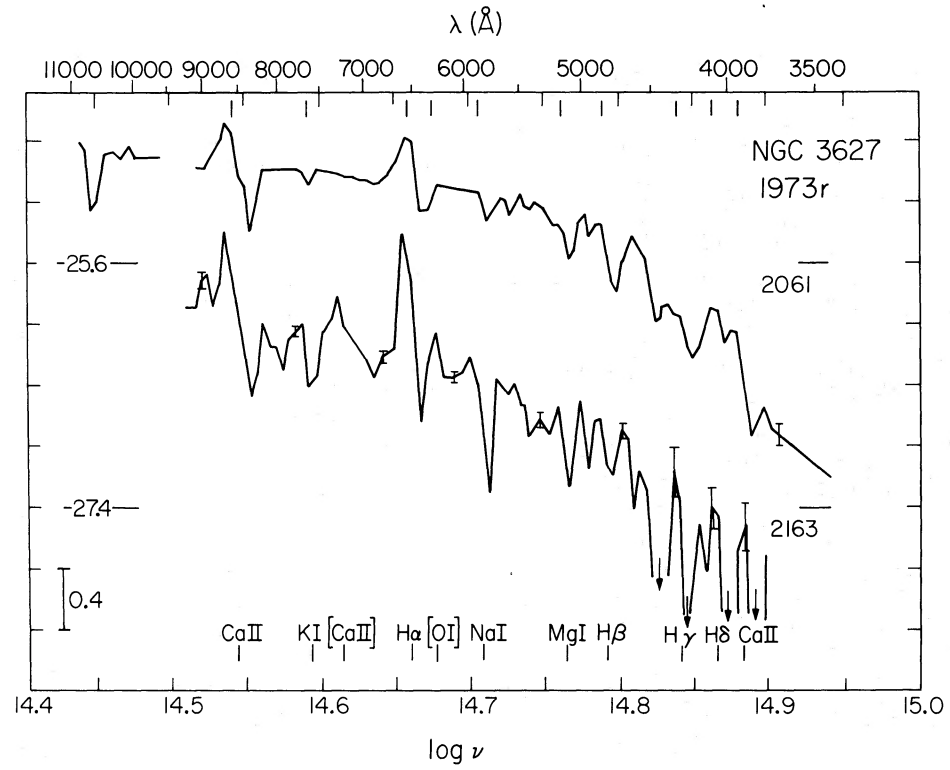

FIG. 1.—Spectrophotometric scans of SN 1973r, in NGC 3627. Log f_ν is plotted against log ν, with the absolute level fixed by the log f_ν at the tick mark on the left of each scan. Error bars indicate the standard deviation only in the regions where errors exceed 0.08 in log f_ν. The last four digits of the Julian date (JD 2,440,000+) are displayed above each scan.

© American Astronomical Society • Provided by the NASA Astrophysics Data System

1975ApJ...197..415K

TABLE 2

PHOTOSPHERIC RADII OF SUPERNOVAE

Supernova and Location	Julian Date (2,440,000+)	Age (days)	Age (s)	T (K)	r(ph) (cm)	Remarks
1969l, NGC 1058.....	591, 600	35	3.0 + 6	6000	1.6 + 15	
	853	293	2.5 + 7	6000?	3.5 + 14	
	1003	443	3.8 + 7	6000??	1.0 + 14	
1970g, M101 (NGC 5457)....	802	2?	1.7 + 5	9500	8.6 + 14	$A_v = 0.44$
	837	37	3.2 + 6	5000	1.7 + 15	
	1056	256	2.2 + 7	5000?	2 + 14	H II region
	1135	335	2.9 + 7	5000?	1 + 14	subtracted
1973r, NGC 3627.....	2061	26	2.3 + 6	5000	1.6 + 15	$A_v = 0.5$
	2163	128	1.1 + 7	5000	3 + 14	

IV. LINE IDENTIFICATION

a) General Considerations

Before discussing the detailed line identifications, it is important to establish the kinematics of the envelope. As is evident from KOPS and figure 1, the shapes of several lines exhibit a definite P Cygni character: blueshifted absorptions balanced by nearly equal emissions centered near the rest wavelength.

This result, in the presence of a strong continuum, suggests that the supernova envelope consists of a photosphere with an expanding atmosphere above it. P Cygni lines are formed by resonant scattering of the photospheric photons by atoms of the expanding gas.

We suppose that all the matter ejected from the supernova expands radially and freely from a central point of explosion. Then the matter at velocity v is a distance $r = vt$ from the center, where t is the time since the explosion. At each point in the envelope, the line opacity is the same along any path and is given by

$$\tau = \frac{hc}{4\pi} BN\left(\frac{r}{v}\right) \cdot \qquad (1)$$

Here B is the Einstein absorption coefficient and N is the number density of atoms in the lower state of the line at the particular point in space. The number density in the upper state of the transition is much smaller and can be neglected. Equation (1) depends on the assumptions that the thermal widths are much smaller than the widths due to mass motions (Castor 1970) and that N varies slowly over a velocity range of the order of the thermal velocity. The escape probability for a photon emitted at a point is

$$\beta = (1 - e^{-\tau})/\tau \, . \qquad (2)$$

These results when combined with knowledge of ionization in the envelope permit a quantitative evaluation of line identifications.

b) Balmer Lines

As shown in figure 1 and KOPS, the emission component of the line at Hα far outweighs the absorption. This net line flux should be due only to recombination in the envelope, as we expect the scattering to have about zero equivalent width and the collisional excitation of Hα is unimportant.

As we will demonstrate, the electron density is 10^{10}–10^{7} cm^{-3}, so that most electrons come from hydrogen, and $n_e = n_{H^+}$. Given the recombination coefficient $\alpha(T)$ from Brocklehurst (1971), we can easily derive $\int n_e^2 dV$ from the number of Hα photons emitted. The volume emitting the hydrogen line, $\int dV$, can be estimated from the velocity of the gas, as measured on the red wing of the emission features, and the time. The results are summarized in table 3, which also gives the rms electron density, $\bar{n}_e$. The uncertainties in these estimates should not amount to more than a factor of 2, except possibly at the late epochs (8 months or more) when the volume is not very well determined. We note that the recombining gas requires a minimum mass of 0.3 $M_\odot$, for the protons alone.

As shown in table 4, the recombination time $(\bar{n}_e\alpha)^{-1}$ is always much less than the age of the supernova envelope. This implies that the hydrogen in the envelope should have recombined far more rapidly than it is observed to do. This subsection shows that reionization from the $n = 2$ level is a plausible mechanism for replenishing the electrons.

Several mechanisms could prevent the electron density from decreasing as fast as the Hα photons are produced. Under some circumstances, photoionization from the ground state is effective, but the dilute radiation from a 5000 K photosphere is far too weak a source of ultraviolet photons. Collisions are even more ineffective in maintaining the electron density over long times.

As illustrated in table 4, the rate of photons emitted shortward of the Balmer limit at λ3648, Q(Balmer), exceeds the recombination rate at early times, and at late times is nearly equal to it. Given the uncertainties in the continuum flux near λ3648, it seems likely that enough photons are produced shortward of the Balmer limit to reionize the hydrogen from $n = 2$ and decrease the rate at which electrons are lost. Under these circumstances, the destruction of a free electron

© American Astronomical Society • Provided by the NASA Astrophysics Data System

1975ApJ...197..415K

TABLE 3

HYDROGEN RECOMBINATION IN SUPERNOVAE

SN	JD (2,440,000+)	v(atm) (cm s^{-1})	R(atm) (cm)	V(atm) (cm^3)	Q(Hα) (s^{-1})	$\alpha(T)$	n_e
1969l.....	600	1 + 9	3.0 + 15	1.1 + 47	2 + 52	5 − 14	2 + 9
	853	5 + 8	1.3 + 16	9.2 + 48	5 + 51	5 − 14	1 + 8
	1003	(4 + 8)	1.5 + 16	1.4 + 49	5 + 50	5 − 14	3 + 7
1970g.....	802	...	1 + 15	4.2 + 45	9 + 51	2 − 14	1 + 10
	837	1 + 9	3.2 + 15	1.4 + 47	2 + 52	5 − 14	2 + 9
	1056	5 + 8	1.1 + 16	5.6 + 48	1 + 51	5 − 14	7 + 7
	1135	5 + 8	1.5 + 16	1.4 + 49	2 + 50	5 − 14	2 + 7
1973r.....	2061	1 + 9	2.3 + 15	5.1 + 46	6 + 51	5 − 14	2 + 9
	2163	5 + 8	5.5 + 15	7.0 + 47	1 + 51	5 − 14	2 + 8

does not occur when it is captured by a proton and cascades to $n = 2$, but only when recombination is followed by de-excitation of the $n = 2$ state. That is:

$$\frac{dn_e(r)}{dt} = n_e^2(r)\alpha\Gamma_{21} \times \left[\frac{\pi r^2(ph)}{r^2}\int_{\nu_0}^{\infty}\frac{B(\nu)}{h\nu}\sigma(\nu)d\nu + \Gamma_{21}\right]^{-1} = -n_2(r)\Gamma_{21}\,, \quad (3)$$

where Γ_{21} is the effective de-excitation rate from $n = 2$ to the ground state, r(ph) is the photospheric radius, r the radius of the point in consideration, $B(\nu)$ the Planck function at the photospheric temperature, and $\sigma(\nu)$ the photoionization cross section from $n = 2$. In this equation we have neglected the effect of expansion on the electron density. We shall denote the integral in equation (3) by $WP\sigma(\nu_0)$, where $\sigma(\nu_0)$ is the threshold photoionization cross section from $n = 2$, W is the geometrical dilution factor $r^2(ph)/r^2$, and

$$P = \pi\int_{\nu_0}^{\infty}[B(\nu)/h\nu][\sigma(\nu)/\sigma(\nu_0)]d\nu$$

is equal to the number of photospheric photons emitted beyond the Balmer limit per second per unit area of the photosphere.

Equation (3) also assumes that the total opacity to ionization from $n = 2$ through the envelope is less than unity. We expect this to be true because, through the era under consideration, we find $WP\sigma \gg \Gamma_{21}$ in the region where Hα is formed. Thus from equation (3), n_2 will be determined by the balance of recombination and reionization. In the early times of expansion, the total number of photons beyond the Balmer limit exceeds the number of Hα photons emitted, so that only a small optical depth in the continuum is required to balance the recombinations with reionizations. At later times, when the number of ionizing photospheric photons decreases, recombinations increase the population of the $n = 2$ level until the continuum optical depth is large enough that reionizations balance the recombinations.

Three possible routes for de-excitation of the $n = 2$ state have been considered: first, collisional de-excitations from $2p$ to $1s$ via electrons; second, $2p$–$1s$ radiative transitions that result in an escaped Lα photon; third, $2s$–$1p$ two-photon decays.

The collisional de-excitation rate can be estimated from the measurements of the excitation cross section made at low energies by Fite (1962). Integrating that cross section with the electron velocity distribution at 5000 K gives an effective rate $C(2p\text{–}1s) = 1.58 \times 10^{-10}\, n_e n_{2p}$ s^{-1}. The escape of Lα is more interesting: the Einstein A is about 6.25×10^8 s^{-1}, but due to the very large optical depth in Lα, the net rate of decays by means of Lα escape is $n_{2p}A_{L\alpha}/\tau_{L\alpha}$. From equation (1) this becomes

$$n_{2p}A_{L\alpha}/\tau_{L\alpha} = \left(\frac{8\pi\nu^3}{c^3}\right)\left(\frac{g_1}{g_{2p}}\right)\left(\frac{1}{t}\right)\left(\frac{n_{2p}}{n_1}\right) = 4.7\left(\frac{10^7}{t}\right)\left(\frac{n_{2p}}{10}\right)\left(\frac{10^9}{n_1}\right). \quad (4)$$

Here the g's are the statistical weights of the states.

TABLE 4

RECOMBINATION TIMES IN SUPERNOVA ENVELOPES

PARAMETER	1969l			1970g				1973r	
	600*	853*	1003*	802*	837*	1056*	1135*	2061*	2163*
t(s).....	3.0 + 6	2.5 + 7	3.8 + 7	(1.7 + 5)	3.2 + 6	2.2 + 7	2.9 + 7	2.3 + 6	1.1 + 7
$1/n_e\alpha$(s).....	1 + 4	2 + 5	7 + 5	5 + 3	1 + 4	3 + 5	1 + 6	1 + 4	1 + 5
Q(Balmer)/Q(Hα).....	2.0	0.4	0.6	44	1.8	0.3	0.9	2.9	0.6
T_d(s).....	2.1 + 7	3.3 + 7	2.0 + 7	...	2.1 + 7	2.0 + 7	1.2 + 7	9 + 6	1.6 + 7
n_2.....	50	6	5	...	48	7	5	100	14
n_1.....	(6 + 8)	9 + 7	6 + 7	...	6 + 8	8 + 7	8 + 7	(8 + 8)	2 + 8
M_H ($M_\odot$).....	(0.3)	1.4	1.1	...	(0.3)	0.7	1.1	(0.1)	0.3

* JD 2,440,000+.

© American Astronomical Society • Provided by the NASA Astrophysics Data System

1975ApJ...197..415K

Two-photon decays from the $2s$ to the $1s$ level have an Einstein A of about 8 s^{-1} (Spitzer and Greenstein 1951). Because $2p$–$2s$ collisions are much more rapid than this decay (Seaton 1955), about one-quarter of the total $n = 2$ population will be in the $2s$ state at any moment. Then, since the emitted photons are not reabsorbed, the net escape rate is about $n_2(A_{2s-1s}/4)$ or $2n_2$ s^{-1}.

From the values of the electron density listed in table 4, we find that collisional de-excitation is always unimportant compared with two-photon decay. Because we do not know n_1, we cannot compare the two-photon decay rate with the Lα decay rate. However, an upper limit on the Lα decay rate permits an estimate of n_1, and hence an estimate of the supernova's mass.

If the picture of reionization from $n = 2$ is correct, the decrease of the electron density and the observed Hα emission must be consistent. From equation (3) we find that the effective decay time of the electrons is

$$T_d = \frac{1}{n_e\alpha}\frac{WP\sigma + \Gamma_{21}}{\Gamma_{21}} . \quad (5)$$

For the reionization process to operate, we require $WP\sigma \gg \Gamma_{21}$ in the region where Hα is formed. As an example, with the photosphere at a radius of 10^{15} cm and at a blackbody temperature of 5000 K, $WP\sigma$ is about 30 at $r = 10^{16}$ cm. With this approximation, we find that a uniform electron decay time throughout the envelope requires $n_e \propto W \propto r^{-2}$. We believe this to be the actual electron distribution. The density distribution of other matter is likely to be steeper than r^{-2}; only the delaying mechanism described here keeps $n_e \propto r^{-2}$.

The density of hydrogen atoms in the $n = 2$ state, n_2, also is proportional to r^{-2}. With this dependence on radius, the number of Hα photons emitted, Q(Hα), the opacity in the Balmer continuum $\tau_{2c}(\nu)$, and the decay time of the electrons, T_d are given by

$$Q(\mathrm{H}\alpha) = [4\pi\alpha n_e^2(R)R^4][1/r(\mathrm{ph}) - 1/R] ; \quad (6)$$

$$\tau_{2c}(\nu) = \frac{\sigma(\nu)\alpha n_e^2(R)R^4}{\sigma(\nu_0)Pr^2(\mathrm{ph})}\left[\frac{1}{r(\mathrm{ph})} - \frac{1}{R}\right] = \frac{\sigma(\nu)Q(\mathrm{H}\alpha)}{\sigma(\nu_0)4\pi r^2(\mathrm{ph})P} ; \quad (7)$$

$$T_d = [1/n_e(R)\alpha][P\sigma(\nu_0)r^2(\mathrm{ph})/\Gamma_{21}R^2] . \quad (8)$$

Here R denotes the outer radius of the envelope. With the estimates of Q(Hα), r(ph), R, and Q(Balmer) from tables 3 and 4, τ_{2c} and T_d can be inferred. Even though the input quantities are not very well determined, the estimate for T_d may be quite good. If at late times we require that τ_{2c} $(\nu_0) = 1$, so that Q(Balmer) = Q(Hα), then the electron decay time is given by

$$T_d = \frac{1}{\Gamma_{21}}\frac{\sigma(\nu_0)}{(4\pi\alpha)^{1/2}}\left\{Q(\mathrm{H}\alpha)\left(\frac{1}{r(\mathrm{ph})} - \frac{1}{R}\right)\right\}^{1/2} . \quad (9)$$

The calculated values of T_d using radiative de-excitation only by means of the two-photon decay, $\Gamma_{21} = 2$ s^{-1}, are presented in table 4. T_d is comparable to the age of the envelope. If we require that the Lα escape rate not exceed 2 s^{-1}, then we can estimate n_1 from equation (4), and thus derive a minimum mass of 1 $M_\odot$ for the supernova envelope. These results are also presented in table 4.

Using

$$\bar{n}_2 = \int_{r(\mathrm{ph})}^{R} n_2 dr/[R - r(\mathrm{ph})]$$

and equation (1), it is straightforward to find the effective optical depth in the Balmer lines. Typically, Hα has $\tau \simeq 300$, but the fact that Lβ is much thicker (τ of order 10^7) means that Hα photons are not converted to Lβ despite numerous scatterings.

The situation is different for Hβ. Optical depths of about 50 in Hβ permit many atoms to reabsorb Hβ photons and return to $n = 4$. There they can either reemit the Hβ, or they can make the 4–3 transition, emitting an optically thin Paschen α, and eventually an Hα. Then the ratio of Hβ photons escaping to Pα photons escaping is just $(A_{42}/\tau_{24})/A_{43}$. Since the Einstein A's are nearly equal, and τ_{24} is estimated to be in the range 30–70, we expect very little Hβ to result from recombination. That explains the very large ratio of Hα/Hβ observed in all the scans. It also has the effect of a modest (30%) increase in the Hα strength at a given electron density, and a twofold increase in the Pα strength.

c) *Lines of* Ca II

Apart from the Balmer lines, the strongest features in the spectra of Type II supernovae about 1 month after maximum light are the features at $\lambda\lambda$3950 and 8600. At times 4 months or more after maximum light, a strong emission feature appears at λ7300. The proposal in KOPS that all of these lines arise from Ca II is explored here in more detail. With the use of an explicit three-level calculation for the calcium ion, the line strengths and line ratios observed are shown to be consistent with the physical conditions of the envelope inferred from Balmer line observations, and with a normal calcium abundance.

Figure 2 illustrates the three lowest energy levels of Ca II. The resonance lines H and K share the same $4p^2\,P$ upper state with the infrared triplet near λ8600. The lower level of the infrared line is the strongly metastable $3d^2D$ level. The forbidden transition $3d^2D$–$4s^2S$ violates the angular-momentum selection rule, and has an Einstein A of about 1 s^{-1} (Osterbrock 1951; Warner 1968). It produces the lines at λ7300: the only other astronomical observation of these lines is in υ Sgr (Greenstein and Merrill 1946).

It is easy to see why these lines could be important features in supernova envelopes. The interpretation of the continuum and the Balmer lines leads to a possible reversing layer consisting of a differentially expanding tenuous mass greater than 1 $M_\odot$, in which the electron density ranges from 10^{10} at early times, to

© American Astronomical Society • Provided by the NASA Astrophysics Data System

1975ApJ...197..415K

TABLE 5

EMISSIVITY OF CALCIUM

JD (2,440,000+)	Observed			Predicted			Best Fit	
	ϵ(8600)	ϵ(7300)	$\frac{Q(8600)}{Q(7300)}$	ϵ(8600)	ϵ(7300)	$\frac{Q(8600)}{Q(7300)}$	$n_{\text{Ca II}}$	$N_{\text{Ca II}}$
1969l:								
600.....	4 + 3	...	>10	3 + 3	1 + 2	35	1 + 3	1 + 50
853.....	3 + 2	2 + 2	1.2	2 + 2	9 + 1	2.0	1 + 3	9 + 51
1003.....	...	5 + 1	...	3 + 1	4 + 1	0.7	6 + 2	8 + 51
1970g								
837.....	3 + 3	...	>10	3 + 3	1 + 2	30	1 + 3	1 + 50
1056.....	6 + 1	8 + 1	0.8	6 + 1	5 + 1	1.2	6 + 2	3 + 51
1135.....	...	3	...	2	3	0.6	6 + 1	8 + 50
1973r:								
2061.....	2 + 4	...	>10	2 + 4	1 + 2	170	5 + 3	3 + 50
2163.....	3 + 2	2 + 2	1.8	3 + 2	1 + 2	2.2	2 + 3	2 + 51

10^7 at the last observations. The gas is irradiated by dilute photospheric flux, with $W = (r_{\text{ph}}/R)^2$ from 10^{-1} to 10^{-4} and T = 10,000–5000 K.

The ionization conditions are adequate to keep nearly all calcium once ionized, but too weak to ionize it further. Because of the relatively high cosmic abundance of calcium (1.66×10^{-6} of hydrogen), and the large populations in the lower levels, large optical depths are present in strong lines. Thus it is not surprising that H and K and the infrared triplet are strong lines at early times. It is also not surprising to see the forbidden line appear after the continuum level has fallen by a factor of 50, with the electron density near 10^7.

We note that as the λ7300 line appears, the λ8600 line loses its absorption trough, and that the number of λ8600 photons produced is about equal to the number of λ7300 photons (table 5). While it is tempting to suppose along with KOPS that, under the proper conditions, absorptions in H and K feed a cascade from 4*p*–3*d*–4*s*, and produce equal numbers of λ8600 and λ7300 photons, this cannot be the correct explanation. The largest possible rate at which photons could be fed into this cascade would be the rate at which H and K photons are removed from the continuum. It is clear from inspecting the figures in KOPS and figure 1 that the photons absorbed at H and K fall far short of the number produced at $\lambda\lambda$8600 and 7300.

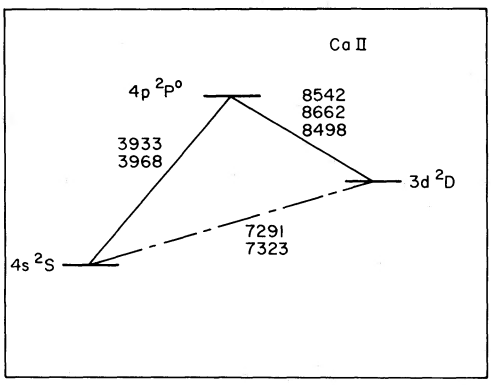

FIG. 2.—Partial Grotrian diagram of the three lowest levels of singly ionized calcium.

We propose here the following explanation for the peculiar ratios of the three Ca II lines. We believe that the $\lambda\lambda$8600 and 7300 emission lines are formed by collisional excitation. The lines H and K are not observed in emission because collisions from the 4*s* to the 4*p* are more often followed by an emission of an 8600 photon than by an H and K photon, due to the large optical depth in H and K. The effective rate of H and K emissions is $A(\text{HK})\beta(\text{HK})$ while for 8600, it is $A(8600)\beta(8600)$. For large optical depths, the branching ratio can be written $A(\text{HK})\tau(8600)/A(8600)\tau(\text{HK})$. As an example, if the ratio of population in the 3*d* to that in 4*s* is Boltzmann at 5000 K, the branching ratio is 0.2.

This argument holds only if the resulting increase in the population of the metastable state is drained away. This condition is met at late times when collisions from the 4*s* to the 3*d* are fast compared with collisions from the 4*s* to the 4*p*, and when the spontaneous decay rate from the metastable state becomes comparable to the rate of collisional de-excitations. We believe the absence of H and K emission at late times is explained by this model.

The nearly equal photon flux from $\lambda\lambda$8600 and 7300 shown in KOPS would then be a coincidence. At later times we expect the photon flux from λ7300 to exceed that from λ8600, as the radiative decays from the metastable state greatly exceed the collisional de-excitations. While both an λ8600 photon and a λ7300 photon are produced by a collision from 4*s* to 4*p*, only a λ7300 photon is produced by a collision from 4*s* to 3*d*. While collisions from the metastable 3*d* to 4*p* would create λ8600 photons without creating λ7300 photons, at late times the population in the 3*d* and the collision rate from 3*d* to 4*p* are so small that very few λ8600 photons are produced this way.

At earlier times the situation is quite different. Then $C(3d\text{–}4s) > A(3d\text{–}4s)$, and the population of the metastable state is fixed at the Boltzmann ratio to the

© American Astronomical Society • Provided by the NASA Astrophysics Data System

1975ApJ...197..415K

ground 4*s* state. The number of λ7300 photons emitted is then fixed, regardless of how much larger the electron density might become. On the other hand, the process of producing λ8600 photons by collisions from 3*d* to 4*p* becomes more important at increasing electron densities. At early times, we expect the number of λ8600 photons to be greater than the number of λ7300 photons.

These general predictions are borne out by comparison of figure 1, JD 2163, at age 4 months; figure 3 of KOPS, JD 135, at age 11 months; and figure 2 of KOPS, JD 003, at age 14 months. At very early times, net emission of λ7300 and of λ8600 is not observed because the strong continuum, and the resultant resonant scattering, mask the contribution from collisions.

To model the processes described above, a numerical solution of the three-level problem has been performed. The differential expansion of the supernova envelope makes this problem particularly easy, as the radiative transfer problem becomes a local one. We use the escape probability formalism of Sobolev (1960) and Castor (1970), and the procedure of Goldreich and Kwan (1974). To illustrate, the rate of population change for the metastable level is

$$\frac{dn_2}{dt} = -n_2[A_{21} + n_e(\gamma_{21} + \gamma_{23})] + n_3(A_{32}\beta_{23} + n_e\gamma_{32}) + n_1 n_e \gamma_{12} . \quad (10)$$

The electron collision cross sections from Burke and Moores (1968) and Petrini (1965) are integrated with the electron energy distribution to obtain excitation and de-excitation rates.

The system of equations is nonlinear because of the dependence of β on the level populations. The equations were solved approximately by an iterative scheme until the accuracy of the solution was adequate. In general, it required only a few steps to produce solutions in which the net flow from one level to another was less than 1 percent of the smallest rate from one level to another by any particular route.

The aim of the calculation was to see whether the observed net rates of photon production in λ8600 and in λ7300 could be reproduced. In practice, it was always possible to match the emissivity (photons cm^{-3} s^{-1}) for one of the lines by adjusting the calcium density. Then the test of whether the model made sense was whether the corresponding emissivity for the other line matched the observations. These calculations were approximate at best because we used an average density of Ca II throughout the envelope, and did not take account of the variation of Ca II density with radius.

The five scans in which the two lines appear, along with the three scans in which only the λ8600 line is significant, are listed in table 5, where the emissivity is tabulated. For the three scans in which only the λ8600 line appears significant, it is difficult to estimate the net emission from the line profile, which is nearly P Cygni. Luckily, accurate values are not necessary at those epochs as our primary aim is to check the λ8600/λ7300 line ratio, and the λ7300 line is not even seen.

The calcium density that gives a rough fit to the λ8600 line is shown in the table. The corresponding λ7300 emissivity is gratifyingly close to the observed values. In the cases where the λ7300 line is much weaker than the λ8600 line, the predictions show the ratio (8600)/(7300) to be 30 or more. In the one intermediate case where the λ8600 line is significantly stronger than the λ7300 line, but are both observed (1973r, JD 2163), the prediction matches the observations very nicely. At late times, the λ7300 line is about as strong as the λ8600 line, and this behavior is reasonably well reproduced by the models. The total number of calcium atoms involved, $\int n(\text{Ca II})dV$, is also tabulated. Since 1 $M_\odot$ at cosmic abundance contains about 2.0×10^{51} calcium atoms, we see that the results are consistent with a normal calcium abundance and an envelope of a few solar masses. The relatively small numbers of calcium ions required for the scans at age 1 month (1969l on JD 600, 1970g on JD 837, 1973r on JD 2061) may reflect the fact that considerable mass is still inside the photosphere at those epochs.

Overall, the understanding of the calcium emission seems satisfactory: the line ratios, which are mostly a function of electron density, are consistent with the electron densities derived from the Hα emission. The line fluxes are consistent with a total amount of calcium that corresponds to a few solar masses at normal calcium abundance.

In the preceding calculation, it was tacitly assumed that all calcium was Ca^+. Here the ionization state of calcium is roughly calculated, and the framework for calculating the ionization of other species is established.

The photoionization rate from a given level can be computed from the integral

$$\gamma = \pi \int_{\nu_0}^{\infty} \sigma(\nu) \frac{B_\nu(T)}{h\nu} d\nu . \quad (11)$$

Taking a sum over the relevant levels provides an estimate of the total photoionization rate, when the geometric dilution of the radiation field is included. Equating the recombination rate to the photoionization rate gives the ionization:

$$\frac{n^+}{n^0} = \frac{\gamma W}{\alpha n_e} = \frac{\gamma}{\alpha}\frac{r^2(\text{ph})}{R^2 n_e(R)} = \frac{\gamma}{\alpha}\frac{r^2(\text{ph})}{R^2 \bar{n}_e}\left\{\frac{3[R - r(\text{ph})]}{r(\text{ph})}\right\}^{1/2} . \quad (12)$$

Here α is the total recombination rate to all levels, and we have assumed $n_e \propto r^{-2}$. Using values from Seaton (1951), the resulting ratios n^+/n^0 are calculated from the values for $\bar{n}_e$, r(ph), and R given in tables 2 and 3, and the results are displayed in table 6. These calculations must underestimate the true amount of ionization because they ignore ionization from upper states.

© American Astronomical Society • Provided by the NASA Astrophysics Data System

1975ApJ...197..415K

TABLE 6

IONIZATION AND OPTICAL DEPTH FOR CALCIUM, SODIUM, AND MAGNESIUM

PARAMETER	1969l			1970g			1973r	
	600*	853*	1003*	837*	1056*	1135*	2061*	2163*
$n_H t$	1 + 17	1 + 16	1 ± 16	8 + 16	1 + 16	7 + 15	1 + 17	6 + 16
Ca^+/Ca^0	2 + 5	7 + 4	3 + 4	2 + 4	6 + 3	5 + 3	3 + 4	1 + 4
$\tau(4226)$	2	4 − 1	1	1 + 1	5	4	1 + 1	2 + 1
Na^+/Na^0	3 + 3	9 + 2	4 + 2	4 + 2	1 + 2	8 + 1	5 + 2	2 + 2
$\tau(5890)$	6 + 1	2 + 1	4 + 1	3 + 2	2 + 2	2 + 2	3 + 2	5 + 2
Mg^+/Mg^0	2 + 2	8 + 1	3 + 1	9	2	2	1 + 1	4
$\tau(5174)$	6 + 1	1	1	1 + 3	5 + 1	3 + 1	2 + 2	1 + 2

* JD 2,440,000±.

The table shows that most calcium will be ionized at least once in the envelope. A similar calculation shows that the ions are not ionized again, despite a second ionization potential of 11.9 eV. Although most of the ionization of Ca^+ to Ca^{++} takes place from the excited states that give rise to the infrared triplet and the forbidden line, consideration of the recombination rate shows that the photoionization does not significantly affect the earlier calculations on the ratios of the three Ca II lines. It is certain that the λλ8600 and 7300 emission at late times does not arise from recombination for two reasons. First, there are too few ionizing photons to supply Ca^{++}, and second, the Hα emission would then be much greater than the λ8600 or λ7300 emission.

d) Lines of Na I, Mg I, Ca I

The identification of the Balmer lines and the three strong Ca II lines accounts for most of the strong features of Type II spectra. No other Ca II or hydrogen lines are expected to be present. The identification of other lines is helped considerably by the physical picture of the envelope developed in the previous sections through the analysis of those lines. Since the electron density, ionizing flux, mass, and total path length are known, it is possible to test guesses about further identifications by calculating the expected optical depth.

After the Balmer lines and the Ca II lines, the next strongest unblended features in the Type II spectra are at λλ5890 and 5180. The first could be either He I λ5876 or Na I λ5890 (the D-lines). The helium identification seems unlikely because none of the other strong triplet lines of He I is seen, and because the lower level ($2p\,^3P$) for that line lies 21 eV above the ground state. As for any line, we can estimate the optical depth:

$$\tau(5876) = \frac{n(2p)}{n(\text{He I})}\,\frac{n(\text{He I})}{n(\text{He})}\,\frac{n(\text{He})}{n(\text{H})}\,\sigma\lambda n_H t\,. \qquad (13)$$

As in all the estimates to follow, if we assume "cosmic" abundance, and a hydrogen density that corresponds to 3 $M_\odot$ in the envelope, we are only required to estimate the ionization and excitation. In the absence of helium ionization, we expect all helium to be He I, and the $2p$ level to be populated no more than the Boltzmann level corresponding to the kinetic temperature. If $T = 5000$ K, the resulting optical depth in λ5876 is astoundingly small—at best 10^{-10}. No other helium line, except λ10830, would be stronger, and λ10830 would still be negligible as long as there is no population of the $2s$ level from above.

We can do a similar calculation for Na I, except that the changes in ionization have to be considered explicitly. The result is shown in table 6: the D-lines have a substantial optical depth at all times, and should be a strong feature through the entire interval under consideration. Thus we conclude that the feature near λ5890 is not He I, but rather Na I. At late times, collisional excitation could lead to emission in the D-lines; however, the small population of Na I compared with Ca II (from table 6) guarantees that emission in the D-lines would be much weaker than in the λλ8600 and 7300 lines of Ca II. No other Na I lines are expected.

Similarly, the feature at λ5180 is likely to be the *b*-lines of Mg I. They arise from the levels $^3P_0$, $^3P_1$, and $^3P_2$, 2.7 eV above the $^1S_0$ ground state. The two levels $^3P_0$ and $^3P_2$ have spontaneous decay rates $\sim 10^{-4}$ s^{-1}, so that for electron densities of 10^4 or more, they will surely be populated at the Boltzmann level for the electron temperature. The $^3P_1$ level has a faster decay rate (~ 430 s^{-1}) and would have a smaller population. Because of the small oscillator strengths of the ^1S–^3P transitions at λ4571, the opacity in that line is much smaller than that in λ5174. For the same reason, collisional excitation of the λ4571 line is slow, and it is not expected in emission. As shown in table 6, the optical depths for Mg I λ5174 are comparable to those for the D-lines. As shown by the scans and by spectra, the *b*-lines remain strong and distinct features throughout the entire period of observation. No other Mg I lines are predicted.

We can use the same method to check whether Ca I at λ4226 should be an important line. As shown in table 6, Ca I could be a line of considerable strength at early times, but the uncertainties in the calculation are too large for a definite prediction. The spectra show no clear evidence for the line, although it could be related to feature 9 of figure 2 in Kirshner and Kwan (1974)

© American Astronomical Society • Provided by the NASA Astrophysics Data System

1975ApJ...197..415K

In these simple cases, where the atomic physics is straightforward, it appears that the method used here is quite successful. It permits a choice between alternative identifications that is based on the physical situation. The lines which are predicted to be strong are strong, and the lines which are expected to be weak are weak.

e) The Feature at λ4600

The strongest feature which has not been identified is the line whose emission peak and absorption trough correspond to a wavelength of λ4600. One possible identification is with the resonance line of Sr I at λ4607. If all strontium were neutral, and the abundance cosmic, this line could have an optical depth of about 10. However, strontium is calcium-like, with an ionization potential of 5.7 eV, so most strontium should be Sr^+. Then the optical depth of the λ4607 line should be much less than 1. The optical depths of the Sr II resonance lines at λλ4078 and 4216 should be of order unity, so it is not surprising that they do not form distinct features. In any event, the Sr II lines would be blended with Hγ and Hδ.

Another possibility for the λ4600 feature is suggested by analogy to other stars with similar physical settings: supergiants, shells around late B stars, and novae near maximum light. The spectrum of Nova Herculis 1934 obtained on the evening of December 13 is illustrated in Stratton's monograph (1936). The line features are much weaker relative to the continuum and are much narrower than in Type II supernovae, but the general character of the spectrum is quite similar to that of 1970g on JD 837. In this spectrum of Nova Herculis, one strong feature is a complex emission band between λ4500 and λ4600, which is produced by transitions in multiplets 37 and 38 of Fe II. These lines, which arise from metastable levels 2.6 eV above the ground state, are also among the strongest features in shell stars. Three other very strong Fe II lines that arise from metastable states about the same height above the ground state are λλ4923, 5018, and 5169 of multiplet 42. Rough estimates of the ionization and populations in these levels show that optical depths of order 100 should be expected. Then it seems very likely that Fe II lines from these multiplets account for the P Cygni features at λ4600, and at λ5000. A similar conclusion based on the absorption features has been reached by Patchett and Branch (1972).

f) Lines of [O I]

In figure 1 and in KOPS, all the observations made 4 months or more after maximum light show some evidence of an emission feature at λ6300. The spectrum of 1969l taken on 1970 August 8 (Kirshner and Kwan 1974) shows this feature distinctly, while the corresponding scan shows it blended with Hα.

A reasonable proposal (KOPS) is that the feature is the [O I] doublet at λλ6300 and 6330. We can test whether this identification is sensible by comparing the observed flux with that expected from an envelope of a few solar masses at 5000 K, with a cosmic oxygen abundance. Because the electron densities of table 4 imply collision rates which are much faster than the radiative rates, the flux we expect to see is given by

$$Q(6300 + 6363) = \frac{n(^1D)}{n(\mathrm{O\ I})}\frac{n(\mathrm{O\ I})}{n(\mathrm{O})}\frac{n(\mathrm{O})}{n(\mathrm{H})} A(^1D - {}^3P) n_{\mathrm{H}} V$$

$$= \frac{g(^1D)}{g(^3P)}\frac{n(\mathrm{O})}{n(\mathrm{H})}\frac{M}{m_{\mathrm{H}}} A(^1D - {}^3P)$$

$$\exp(-2.27 \times 10^4\, T).$$

For $T = 5000$ K, and $n(\mathrm{O})/n(\mathrm{H}) = 6.76 \times 10^{-4}$,

$$Q(6300 + 6363) = 4.3 \times 10^{+49}\, M/M_\odot \text{ photons s}^{-1}.$$

We note that this is an upper limit to the photon flux: unless there is some means of population from above, the population in the ^1D level cannot exceed the assumed amount. Also, the photon flux should remain roughly constant, as long as the electron density is high enough ($n_e > 10^5$).

The scans show that about 1×10^{50} photons per second are emitted by 1973r on JD 2163, and about the same values for 1969l on JD 1003, and 1970g on JD 1135. This photon flux corresponds to the emission from about 2 or 3 $M_\odot$ at the usual oxygen abundance. It is interesting that the photon flux for 1973r, only 5 months after maximum light, is comparable to the flux from 1969l almost 15 months after maximum. This seems to support the idea that emission at both early times and late is proceeding at the maximum allowable rate.

The largest photon flux at λ6300 comes from the scan of 1970g in M101 on JD 1056. There we see about 5×10^{50} photons per second, corresponding to emission from about 10 $M_\odot$. Although the supernova in M101 erupted in an H II region, the O I flux from the surrounding gas has been subtracted from the supernova observations.

g) Other Lines

With a knowledge of the ionization conditions and the mechanism of line formation, it is possible to check systematically for other possible line identifications, both in emission and in absorption.

Some possibilities in emission include C I λ8727, and S I λ7726. Both of these are low-lying forbidden lines of abundant elements that would be neutral. The photon flux from carbon probably could not exceed 1×10^{50} photons s^{-1}. This is comparable to the strength of O I, and could be significant at late epochs, although it would appear blended with λ8600 from Ca II at low resolution. The photon flux from the sulfur line might attain 2×10^{49} s^{-1}, and may be related to the very small emission seen in 1973r on JD 2163 (fig. 1).

Potassium has two lines which can arise from the ground state, at λ7677 and at λ4045. Potassium is ionized at early epochs, but the line could attain τ of 100 after a few months. The scan of 1973r (JD

© American Astronomical Society • Provided by the NASA Astrophysics Data System

1975ApJ...197..415K

2163) shows two absorption features at the correct wavelengths; however, the atmospheric A-band of O_2 introduces some uncertainty at λ7677, while the blue-shifted absorption from Hδ would blend with λ4045. Thus the presence of potassium is not proven, but seems a good possibility.

V. SUMMARY

Most of the features of Type II spectra can be understood in terms of an expanding atmosphere of 2–5 $M_\odot$ with cosmic abundance. Hydrogen recombination is slowed by reionization from the $n = 2$ level by photospheric photons in the Balmer continuum. The net leakage from $n = 2$ is probably by means of two-photon decay, if the supernova envelope has at least 1 $M_\odot$ to prevent the easy escape of Lα. The opacity in Hβ accounts for the large Hα/Hβ ratio.

The interesting behavior of the Ca II emission lines can be understood in some detail, if the electron densities derived from the hydrogen recombination are correct, and if the envelope has a mass of about 3 $M_\odot$ with a cosmic calcium abundance.

Under the same assumptions, the strong lines of Na I and Mg I can be easily accounted for. The features at λ5000 and at λ4600 can probably be attributed to Fe II, and the [O I] line has the expected strength.

These threads of evidence seem so consistent that one can have considerable confidence that this simple view of the overall situation is correct.

We are grateful for the data, ideas, and encouragement provided by J. B. Oke, A. R. Sandage, J. L. Greenstein, L. Searle, and J. E. Gunn. R. P. K. is a Virginia Steele Scott Fellow. J. K.'s research is sponsored by National Science Foundation grant GP-40768x.

REFERENCES

Barbon, R., Ciatti, F., and Rosino, L. 1973, *Astr. and Ap.*, **29**, 57.
Burke, P. G., and Moores, D. L. 1968, *Proc. Phys. Soc. (London)*, *B*, **1**, 575.
Brocklehurst, M. 1971, *M.N.R.A.S.*, **153**, 471.
Castor, J. I. 1970, *M.N.R.A.S.*, **149**, 111.
Ciatti, F., Rosino, L., and Bertola, F. 1971, *Mem. Soc. Astr. Ital.*, **42**, 163.
Fite, W. L. 1962, in *Atomic and Molecular Processes*, ed. D. R. Bates (New York: Academic Press), Chap. 12.
Goldreich, P., and Kwan, J. 1974, *Ap. J.*, **189**, 441.
Greenstein, J. L., and Merrill, P. W. 1946, *Ap. J.*, **104**, 177.
Kirshner, R. P., and Kwan, J. 1974, *Ap. J.*, **193**, 27.
Kirshner, R. P., Oke, J. B., Penston, M., and Searle, L. 1973, *Ap. J.*, **185**, 303 (KOPS).
Oke, J. B. 1969, *Pub. A.S.P.*, **81**, 11.
Oke, J. B., and Schild, R. E. 1970, *Ap. J.*, **161**, 1015.
Osterbrock, D. E. 1951, *Ap. J.*, **114**, 469.
Patchett, B., and Branch, D. 1972, *M.N.R.A.S.*, **158**, 375.
Petrini, D. 1965, *Compt. Rend.*, **260**, 4929.
Seaton, M. J. 1951, *M.N.R.A.S.*, **111**, 368.
———. 1955, *Proc. Phys. Soc. (London) A*, **68**, 457.
Sobolev, V. V. 1960, *Moving Atmospheres of Stars* (Cambridge: Harvard University Press).
Spitzer, L., and Greenstein, J. L. 1951, *Ap. J.*, **114**, 407.
Stratton, F. J. M. 1936, *Ann. Solar Phys. Obs. Cambridge*, Vol. **4**, Pt. 4.
Warner, B. 1968, *M.N.R.A.S.*, **139**, 115.

ROBERT P. KIRSHNER: Kitt Peak National Observatory, P.O. Box 26732, Tucson, AZ 85726

JOHN KWAN: Department of Earth and Space Sciences, State University of New York, Stony Brook, NY 11794

© American Astronomical Society • Provided by the NASA Astrophysics Data System